Supplementary Materials

Nitrogen and oxygen-codoped dense porous carbon enhancing ion adsorption for high-volumetric performance supercapacitors

Yaoyao Chen[1,#], Zhen Wang[2,#], Xueli Mei[1,3], Qunying Wang[4], Hongtao Xie[1,*], Yizhao Li[1,3,*]

[1]Huzhou Key Laboratory of Smart and Clean Energy, Yangtze Delta Region Institute (Huzhou), University of Electronic Science and Technology of China, Huzhou 313001, Zhejiang, China.
[2]Strait Institute of Flexible Electronics (SIFE, Future Technologies), Fujian Key Laboratory of Flexible Electronics, Fujian Normal University and Strait Laboratory of Flexible Electronics (SLoFE), Fuzhou 350117, Fujian, China.
[3]State Key Laboratory of Chemistry and Utilization of Carbon Based Energy Resources, College of Chemical Engineering and Technology, Xinjiang University, Urumqi 830046, Uygur Autonomous Region of Xinjiang, China.
[4]Huadian Electric Power Research Institute Co., Ltd., Hangzhou 310030, Zhejiang, China.
[#]These authors made equal contributions to this work.

Correspondence to: Dr. Hongtao Xie, Huzhou Key Laboratory of Smart and Clean Energy, Yangtze Delta Region Institute (Huzhou), University of Electronic Science and Technology of China, No. 819, Xisaishan Road, Huzhou 313001, Zhejiang, China. E-mail: xieht@csj.uestc.edu.cn; Prof. Yizhao Li, Huzhou Key Laboratory of Smart and Clean Energy, Yangtze Delta Region Institute (Huzhou), University of Electronic Science and Technology of China, No. 819, Xisaishan Road, Huzhou 313001, Zhejiang, China. E-mail: yizhao@csj.uestc.edu.cn

Supplementary Note S1. Electrochemical characterization

Working electrodes were fabricated by coating a mixture with a mass ratio of 85:10:5, consisting of the samples, acetylene black, and poly(tetrafluoroethylene) (PTFE) binder onto nickel foam (for aqueous electrolytes) or stainless steel mesh (for organic electrolytes) as current collectors. The average loading of active materials was approximately 2 mg cm^{-2}. Three-electrode measurements were conducted in a 6 mol L^{-1} KOH aqueous electrolyte, while two-electrode tests were performed in both aqueous and organic electrolytes (1 mol L^{-1} tetraethylammonium tetrafluoroborate ($TEABF_4$)). Cyclic voltammetry (CV) and galvanostatic charge-discharge (GCD) curves were recorded using a CHI760E electrochemical workstation (Shanghai Chenhua Instrument Co. Ltd., China). Electrochemical impedance spectroscopy (EIS) analyses were carried out within a frequency range of 0.01 Hz to 100 kHz, with an amplitude of 5 mV.

In the three-electrode system, the specific gravimetric capacitances (C_g, F g^{-1}) and volumetric capacitance (C_v, F cm^{-3}) were calculated from galvanostatic discharge curves with the voltage window of -0.9−0.1 V based on

$$C_g = I\,\Delta t \,/\, m\,\Delta V \quad (1)$$

$$C_v = C_g \times \rho \quad (2)$$

$$\rho = m / V \quad (3)$$

here, I represents the discharge current (A), Δt denotes the discharge time (s), m corresponds to the mass of the active material (g), ΔV indicates the voltage range (V), ρ refers to the compaction density of the active material (g cm^{-3}), while m and V represent the mass (g) and volume (cm^3) of the sample, respectively. The volume of the active material was determined by measuring the radius (r) and thickness (h) of the compressed active material under a pressure of 10 MPa in a cylindrical mold, using $V = h \times \pi \times r^2$.

In the two-electrode system, the CV and GCD measurements were performed over a voltage range of 0−1 V in aqueous electrolyte and 0−2.5 V in organic electrolyte. The specific gravimetric capacitance C_s (F g^{-1} / F cm^{-3}), the energy density (E, Wh kg^{-1}) and the power density (P, W kg^{-1}) were calculated according to

$$C_s = 4\,I\,\Delta t \,/\, m\,\Delta V \quad (4)$$

$$E = C_s\,(\Delta V)^2 \,/\, 8 \times 3.6 \quad (5)$$

$P = 3600\ E / \Delta t$ (6)

where C_s is the gravimetric/volumetric capacitance (F g^{-1} / F cm^{-3}) of the symmetric system, ΔV is the voltage window (V) excluding the *IR* drop, and Δt is the discharge time (s).

The ion transmission coefficient (σ) was calculated by

$$\sigma = \frac{RT_0}{n^2F^2A\sqrt{2}}\left(\frac{1}{D^{0.5}C^*}\right) \quad (7)$$

where T_0 is the absolute temperature, R is the gas constant, F is the Faraday constant, n is the charge-transfer number, A is the area of interfacial electrode/electrolyte and C^* is the concentration of electrolyte. The parameter D manifests the interaction force at the NDPC/electrolyte interface.

Supplementary Note S2. Compaction density test and measurement methods

The compaction density test of the material was conducted by placing the powder sample into a cylindrical die with a diameter (*r*) of 13 mm, followed by the application of a uniaxial mechanical pressure of 10 MPa to compress the sample. The resulting height (*h*, cm) of the compacted pellet was then measured.

$V = h \times \pi \times r^2$ (8)

$\rho = m / V$ (3)

Supplementary Note S3. DFT calculation methods

DFT calculations were performed using the Quantum ESPRESSO, coupled with the generalized gradient approximation of the Perdew-Burke-Ernzerhof for the exchange correlation functional. The models for the pure carbon (C) and N/O co-doped C were modeled based on XPS analysis. The interaction of ion-electron is described by projected augmented wave. The Kohn-Sham orbitals were expanded in a plane-wave basis set with a kinetic energy cutoff of 30 Ry and a charge-density cutoff of 300 Ry. The Fermi surface effects have been treated by the smearing technique of Methfessel and Paxton, using a smearing parameter of 0.02 Ry. The Brillouin zones were sampled with a k-point mesh of 1 × 1 × 2. The two slab models including pure C and N/O co-doped C were constructed with a vacuum space of 16 Å and 5 × 5 × 1 lateral periodicity. The adsorption energy (E_{ad}) of electrolyte ions is calculated by

$$E_{ad} = E_{compound} - E_K - E_{str} \quad (9)$$

where $E_{compound}$ is the total energy of the structure and K ion, E_K is the energy of K ion, and E_{str} is the energy of corresponding structure.

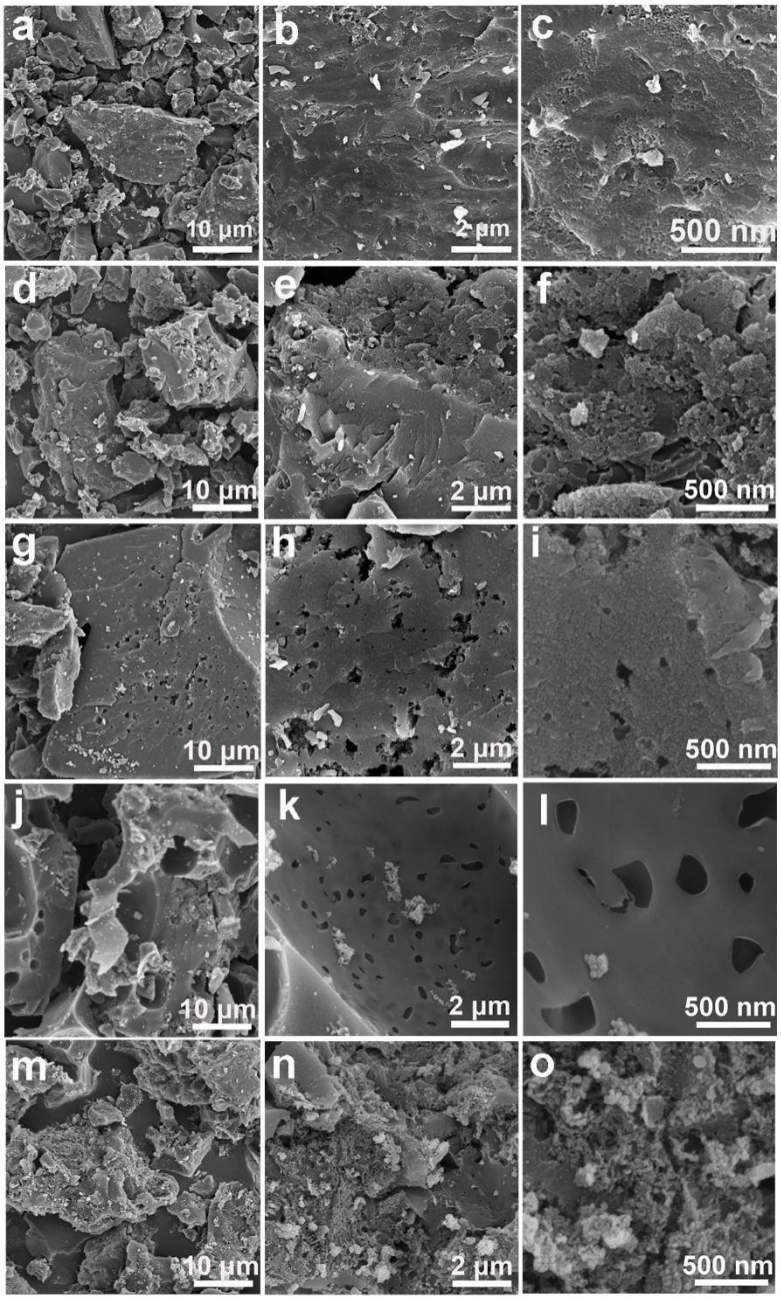

Supplementary Figure S1. SEM images of NDPCs: (a-c) DPC, (d-f) NDPC-0.25, (g-i) NDPC-0.5, (j-l) NDPC-0.75 and (m-o) NDPC-1.

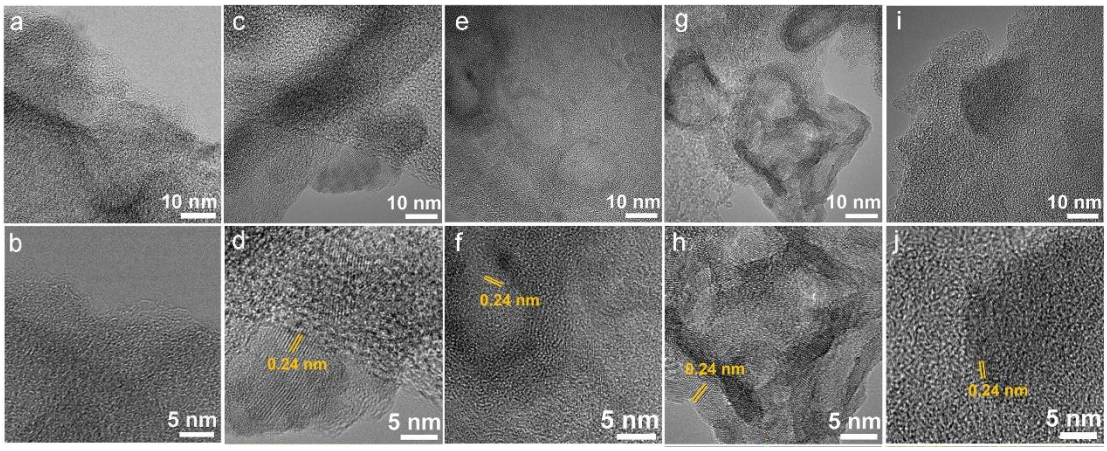

Supplementary Figure S2. HRTEM images of NDPCs: (a-b) DPC, (c-d) NDPC-0.25, (e-f) NDPC-0.5, (g-h) NDPC-0.75 and (i-j) NDPC-1.

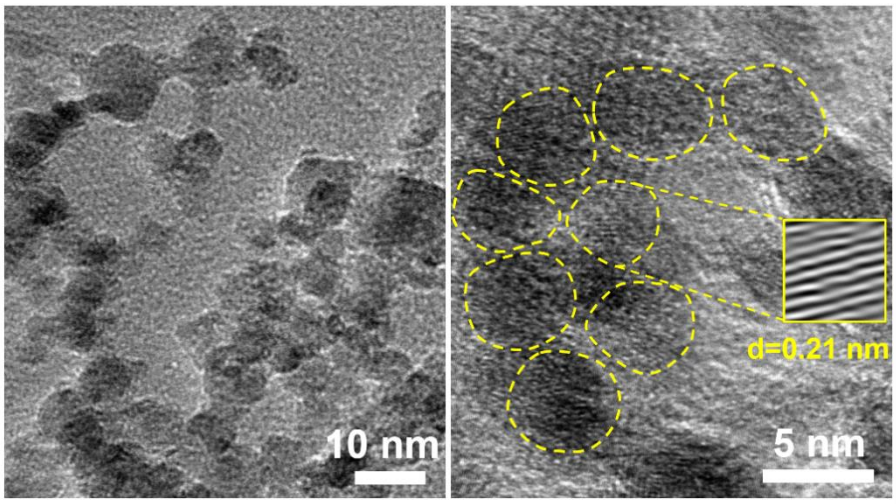

Supplementary Figure S3. HRTEM images of the CDs.

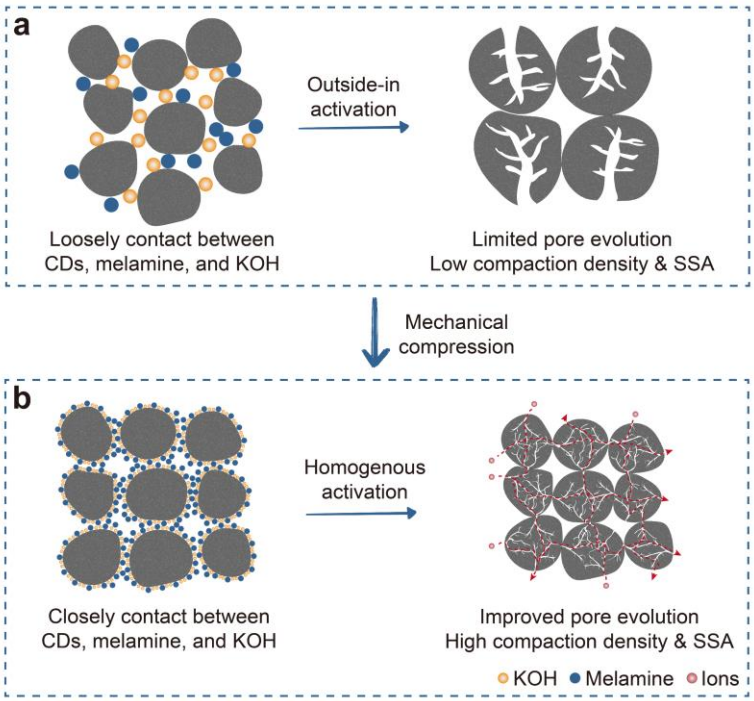

Supplementary Figure S4. Schematic of the porous structure development through different activation processes.

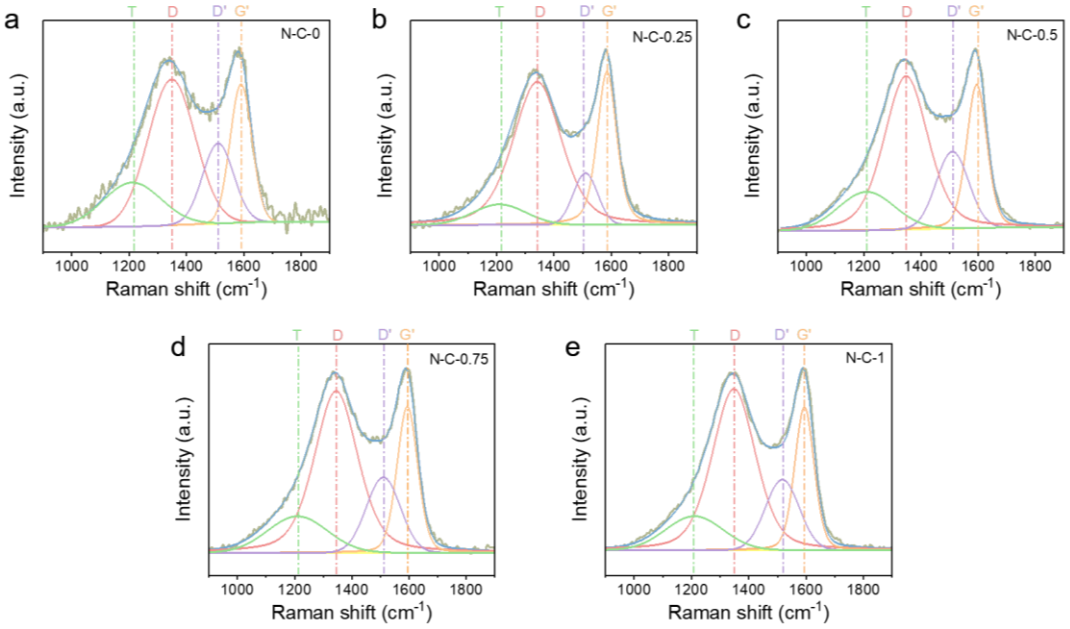

Supplementary Figure S5. Raman spectra of (a) DPC, (b) NDPC-0.25, (c) NDPC-0.5, and (d) NDPC-0.75, (e) NDPC-1.

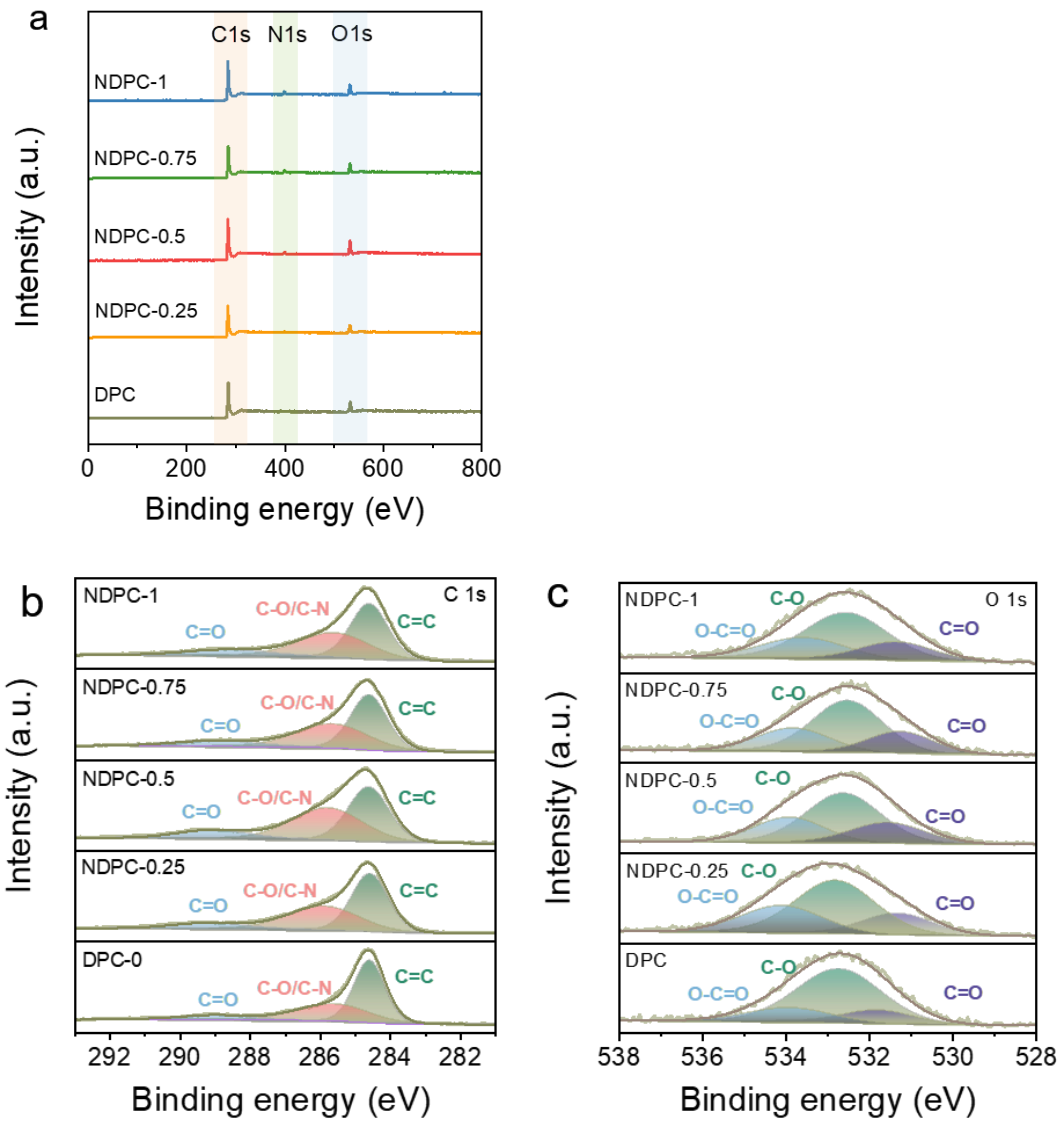

Supplementary Figure S6. The (a) XPS survey, (b) XPS C 1s spectra, (c) XPS O 1s spectra of DPC and NDPCs.

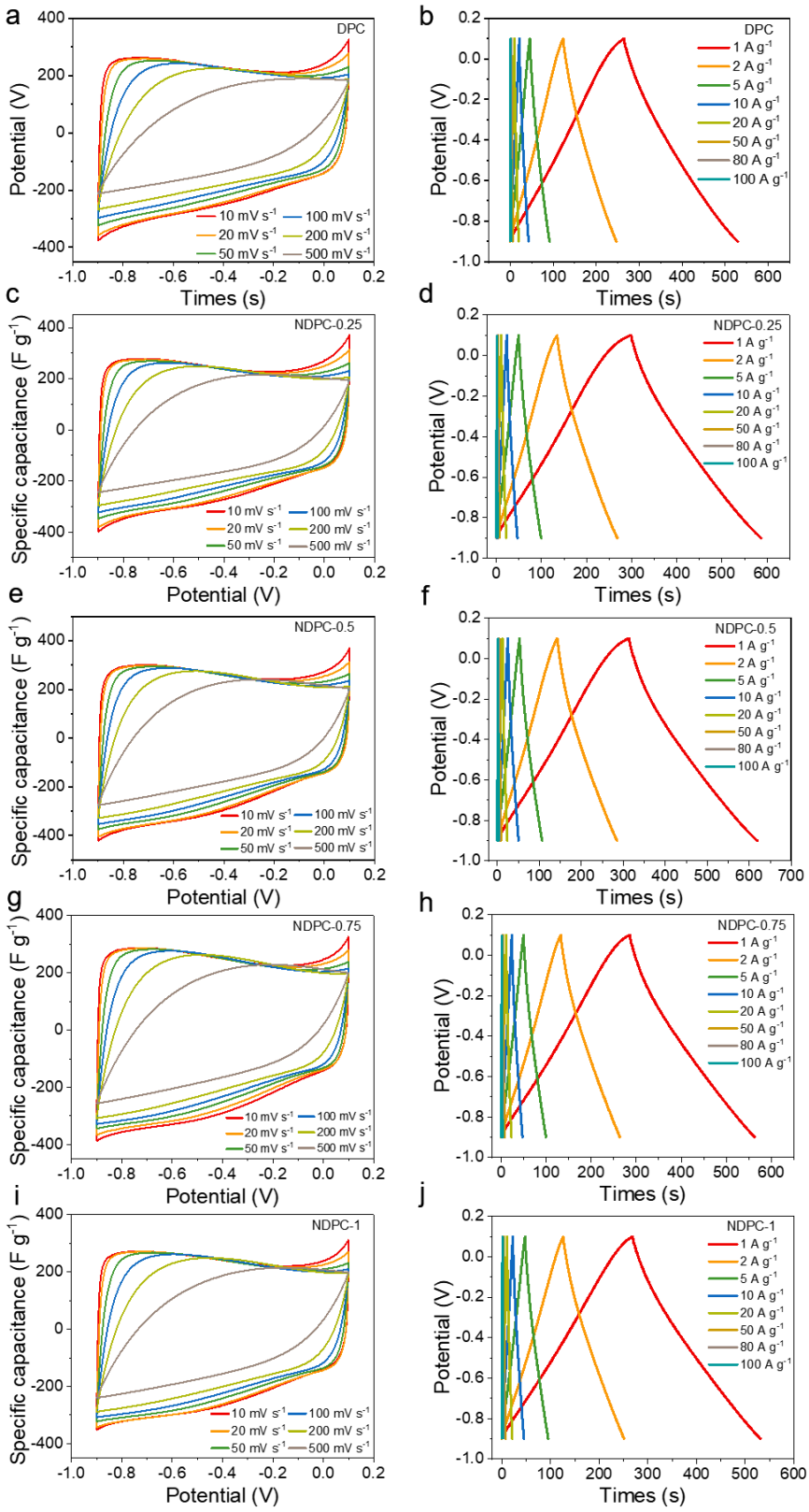

Supplementary Figure S7. CV curves at different scan rates and GCD curves at different current densities of the (a, b) DPC, (c, d) NDPC-0.25, (e, f) NDPC-0.5, (g, h) NDPC-0.75, and (i, j) NDPC-1 in three-electrode system.

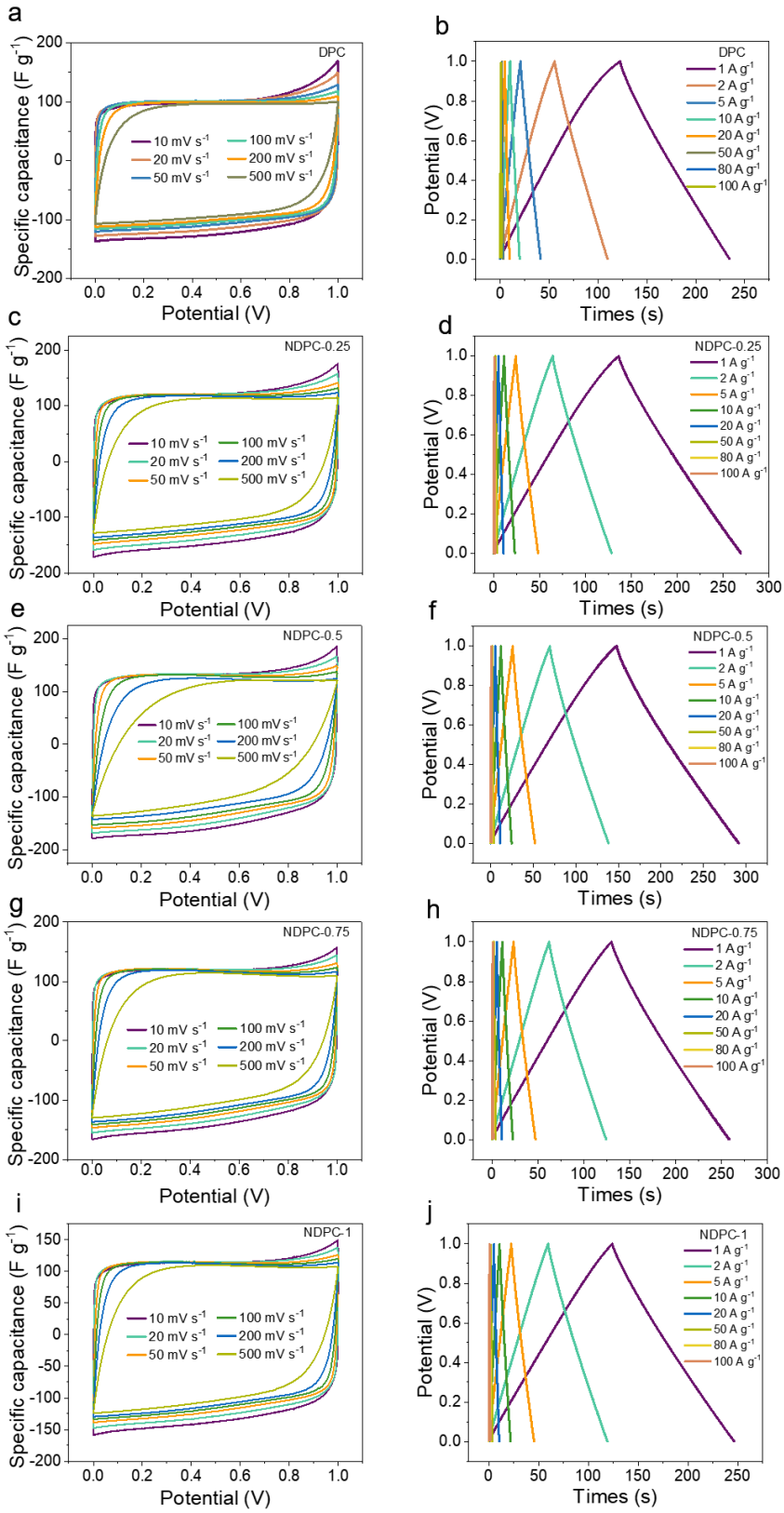

Supplementary Figure S8. (a) CV curves at different scan rates and GCD curves at different current densities of the (a, b) DPC, (c, d) NDPC-0.25, (e, f) NDPC-0.5, (g, h) NDPC-0.75, and (i, j) NDPC-1 in two-electrode system.

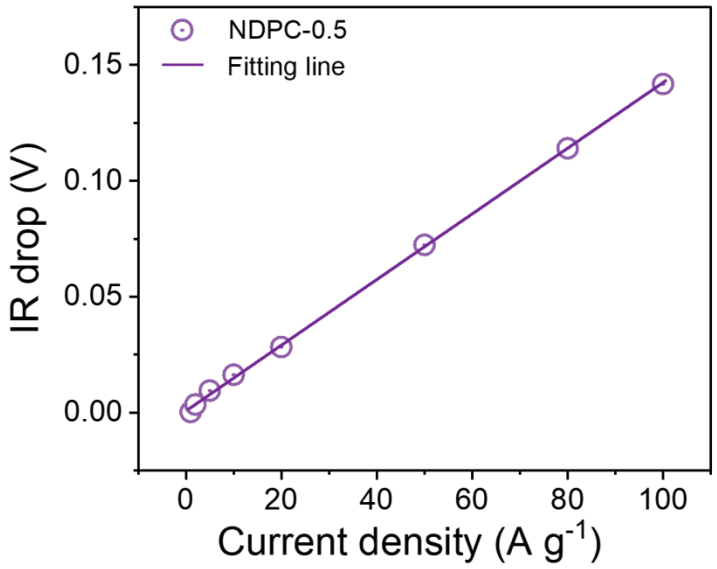

Supplementary Figure S9. IR drop of NDPC-0.5.

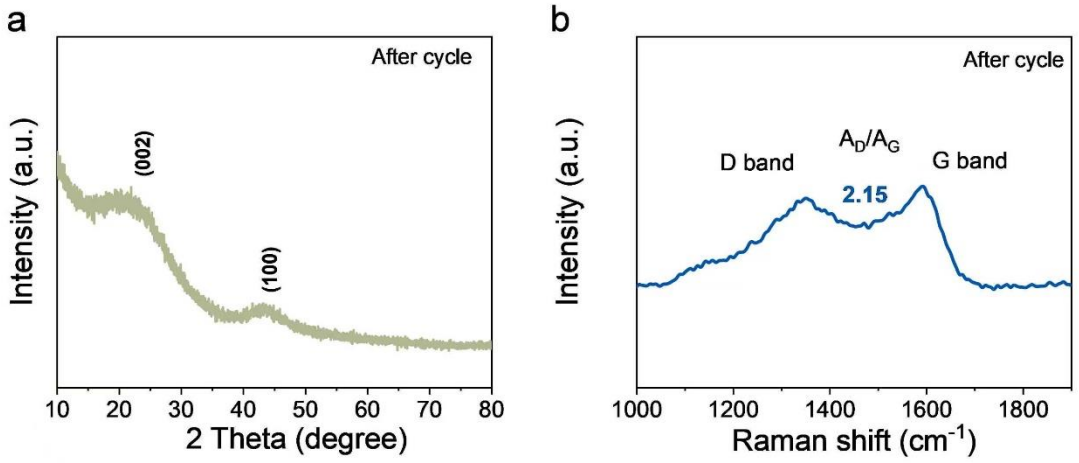

Supplementary Figure S10. a XRD curve and b Raman curve of NDPC after cycling.

Supplementary Table S1. Texture properties of the NDPCs measured by N_2 adsorption-desorption isotherms.

Samples	S_{BET}[a] ($m^2\ g^{-1}$)	V_{total}[b] ($cm^3\ g^{-1}$)	V_{micro}[c] ($cm^3\ g^{-1}$)	V_{meso}[d] ($cm^3\ g^{-1}$)	Compaction density ($g\ cm^{-3}$)
DPC	1359	0.62	0.43	0.19	0.97
NDPC-0.25	1527	0.77	0.64	0.13	1.21
NDPC-0.5	1756	0.88	0.63	0.25	1.19
NDPC-0.75	1437	0.75	0.36	0.39	1.03
NDPC-1	1395	0.73	0.25	0.48	0.95

[a] Specific surface area calculated by BET method.

[b] Total pore volume.

[c] Volume of micropores.

[d] Volume of mesopores.

Supplementary Table S2. Yield of NDPCs.

Sample	Yield (wt.%)
NDPC-0	30.4
NDPC-0.25	44.5
NDPC-0.5	47.2
NDPC-0.75	53.1
NDPC-1	61.8

Supplementary Table S3. Concentration of carbon and oxygen in the samples from XPS survey spectra, and contribution of the components in the area of the XPS C 1s spectra.

Samples	Element composition (%)			Contribution of the components in C 1s spectra (%)		
	C	O	N	C=C	C−O	C=O
DPC	88.5	11.5	--	55	35	10
NDPC-0.25	86.7	11.1	2.2	50	40	10
NDPC-0.5	83.3	13	3.7	44	44	12
NDPC-0.75	82.5	11.4	6.1	48	41	11
NDPC-1	81.6	10.7	7.7	48	40	12

Supplementary Table S4. Contribution of the components in the area of the XPS O 1s spectra and N 1s spectra.

Samples	Contribution of the components in O 1s spectra (at. %)			Contribution of the components in N 1s spectra (at. %)			
	C=O	C−O	O−C=O	N−6	N−5	N−Q	N−O
DPC	2.8	6.9	2.9	--	--	--	--
NDPC-0.25	2.2	5.9	3.0	0.8	0.8	0.3	0.3
NDPC-0.5	2.9	6.9	3.2	1.0	1.6	0.7	0.4
NDPC-0.75	2.5	6.1	2.8	2.3	2.5	0.8	0.5
NDPC-1	2.2	5.8	2.7	3.0	3.2	0.9	0.6